Turbulence Structure and Scalar Transfer in Stratified Free-Surface Flows

Ryuichi Nagaosa and Takayuki Saito
Mining and Geophysical Dept., National Institute for Resources and Environment, Tsukuba 305, Japan

Direct numerical simulations were used to investigate turbulence structure and scalar transfer across a shear-free, nonwavy gas-liquid interface (free surface) in stably stratified turbulent flows. These simulations solve the Navier–Stokes and thermal-energy conservation equations, using a finite difference approximation. The relation between the turbulence structure in the stably stratified turbulent boundary layer and organized motion near the free surface are discussed. In addition, scalar transfer across a free surface is investigated by solving a passive scalar conservation equation after both velocity and temperature fields are fully developed. The effects of stable stratification on the scalar transfer process in a region very close to the free surface are also discussed.

Introduction

Scalar transfer in turbulent flows across a gas–liquid interface is of great interest in areas such as chemical engineering and geophysics. Resistance against the scalar transfer across the gas–liquid interface mainly exists in the liquid phase, since molecular diffusivity in the liquid phase is much smaller than that in the gas phase. For example, the ratio between molecular Prandtl numbers in the liquid and gas phases is about 7.20 in pure water at 293 K and 101.3 kPa. This fact suggests that the turbulence structure below the gas–liquid interface may play an important role in the scalar transfer across the gas–liquid interface. Therefore, many researchers have studied the details of turbulence structure below the gas–liquid interface to clarify the scalar transfer mechanism.

Based on several experiments, some knowledge about scalar transfer across the gas–liquid interface has been gained. Dankwerts (1951) proposed the theoretical surface-renewal model to describe the mechanism of gas absorption. Although this model is dated, it is still widely accepted. Fortesque and Pearson (1967) conducted a numerical analysis of a scalar transfer equation to estimate the scalar transfer rate into a turbulent flow. In addition, they presented a correlation between the turbulence intensity near the free surface and the scalar transfer coefficient based on the large-scale surface-renewal modeling. Komori et al. (1982, 1989, 1990) carried out measurements of turbulence structures and the scalar transfer coefficient across the gas–liquid interface. Their results indicate that the scalar transfer coefficient across the gas–liquid interface depends only on the frequency of large-scale surface-renewal eddies. Rashidi et al. (1990, 1991) investigated gas–liquid two-phase coupled turbulence and visualized the turbulence structure by means of the microbubble tracers technique. They also measured the frequency of patchlike well-organized eddies near the interface.

Recently, direct numerical simulation (DNS) has become a significant tool for analyzing transport phenomena in turbulent flows. DNS is particularly useful when simultaneous measurements of instantaneous velocity and scalar fields are required. Lam and Banerjee (1992) conducted the first DNS of free-surface flows with flat gas–liquid interface using a pseudospectral method. They clarified the formation of the streaky structures and details of the turbulence statistics with and without interfacial shear stress. Understanding the formation of these streaks in the turbulent boundary layer is one of the key points in clarifying the scalar transport process, since a large part of the turbulence energy is generated in the turbulent boundary layer. Komori et al. (1993) presented DNS of shear-free gas–liquid interface (free surface) based on a boundary-fitting finite difference method on semi-Lagrangian curvilinear coordinates. Their results showed that the well-organized bursting eddies are lifted up from the near-wall region and renew the free surface as surface-renewal eddies.

Correspondence concerning this article should be addressed to R. Nagaosa.

Handler et al. (1993) found the existence of surface-attached vortical structures in the free-surface turbulence. They also estimated the characteristic velocity and length scale near the free surface. These estimations will be required in establishing subgrid scale models of free-surface turbulence for large-eddy simulations (LES). Pan and Banerjee (1995) investigated details of the vortical structure near the free surface in both steady and freely decaying turbulence, and details of the vorticity evolution were carefully investigated.

The turbulence structure near the free surface is considerably affected when an active scalar (e.g., thermal energy) is transferred across the free surface. According to previous reports (Komori et al., 1983; Gerz et al., 1989; Holt et al., 1992), the distribution of turbulence statistics in stably stratified flows depends on the local Richardson number, defined by the local velocity and temperature gradients (see Eq. 10 in this article). These results suggest that the effect of thermal stratification is significant in the scalar transfer into turbulent flows. The turbulence structure and scalar transfer near the free surface in stratified flows are complicated since the stratification influences the turbulence structure, especially in the turbulent boundary layer near a rigid bottom wall. Unfortunately turbulence structures of a thermally stratified turbulent boundary layer have not been studied in the previously published articles. The presence of a wall (viscous or inviscid) makes the vorticity evolution in the turbulent boundary layer much more complicated due to the blocking effects of the wall. Therefore, the influence of the thermal stratification on the scalar transfer across the free surface is still not well known. From this point of view, studies of the details of the turbulence structures and scalar transfer mechanisms in stably stratified flows are necessary, for example, to establish subgrid scale models for thermally stratified wall turbulence.

The purpose of this study is to investigate the relationship between turbulence structures and the scalar transfer mechanism in both unstratified and stratified free-surface turbulence. For simplicity, only stably stratified free-surface turbulence is described in this article. Direct numerical simulation is used to obtain the turbulent flows with free-surface. In addition to these simulations of the governing equations, the unsteady passive scalar transfer equation is simultaneously solved after both velocity and temperature fields are fully developed to study the scalar transfer mechanism across the free-surface.

Numerical Procedure

Problem setup

The flow configuration is shown in Figure 1. Subscripts 1, 2 and 3 indicate the streamwise, spanwise, and vertical directions. Fully developed turbulent flows with or without stable stratification are bounded by a viscous (bottom) wall and an inviscid (top) wall.

The boundary conditions for the velocity and temperature on both walls are shown:

$$\begin{aligned} u_1 = u_2 = u_3 = 0 \quad &\text{and} \quad T = 0 \quad \text{at} \quad x_3 = 0 \\ \frac{\partial u_1}{\partial x_3} = \frac{\partial u_2}{\partial x_3} = u_3 = 0 \quad &\text{and} \quad T = \Delta T \quad \text{at} \quad x_3 = \delta. \end{aligned} \tag{1}$$

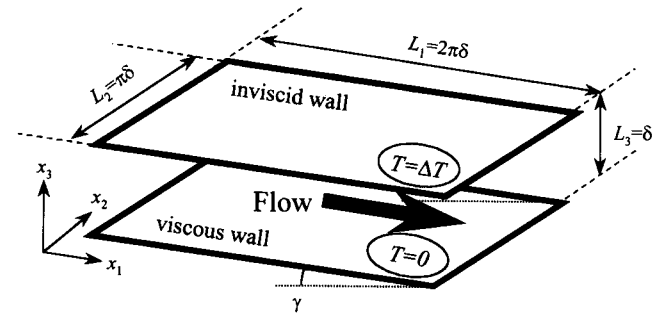

Figure 1. Configuration of free-surface flows.

The temperature difference between the top and bottom walls, ΔT (> 0), exists to impose a stable stratification. According to Komori et al. (1993), the deformation of the free surface at low Reynolds and Froude numbers is about 50 μm toward a 5-cm water depth. This negligibly small amplitude of surface deformation justifies the assumption that the boundary condition on the free surface can be simplified to a free-slip condition. Periodic boundary conditions are used for all dependent variables in both streamwise and spanwise directions. The flows between the two parallel walls are driven by a pressure gradient caused by the gravitational force. The friction velocity on the bottom wall is expressed by this equation,

$$u_\tau = (\delta g \sin\gamma)^{1/2}. \tag{2}$$

The sizes of the computational domain, L_1, L_2, and L_3 are $2\pi\delta$, $\pi\delta$, and δ in the streamwise, spanwise, and vertical directions, which correspond to 943, 471, and 150 in wall units. The sizes of the computational domain are large enough to assume that the flow is periodic in both the streamwise and spanwise directions (Jiménez and Moin, 1991).

Governing equations

We assumed that the fluid is incompressible and Newtonian with constant physical properties. The governing equations in the nonisothermal system are

$$\frac{\partial u_i}{\partial x_i} = 0, \tag{3}$$

$$\frac{\partial u_i}{\partial t} = -\frac{\partial p}{\partial x_i} - \frac{\partial}{\partial x_j} u_j u_i + \frac{1}{Re}\frac{\partial^2 u_i}{\partial x_j \partial x_j} + RiT, \tag{4}$$

$$\frac{\partial T}{\partial t} = -\frac{\partial}{\partial x_j} u_j T + \frac{1}{RePr}\frac{\partial^2 T}{\partial x_j \partial x_j}. \tag{5}$$

The Boussinesq approximation is used to express the buoyancy term. These equations are already normalized by the water depth, δ, the friction velocity, u_τ, and the temperature difference, ΔT. After the normalization, three dimensionless parameters appear in the governing equations;

$$Re = \frac{\delta u_\tau}{\nu}, \qquad Pr = \frac{\nu}{\alpha}, \qquad Ri = \frac{\beta g \delta \Delta T}{u_\tau^2}, \tag{6}$$

The Reynolds number (Re) used in this study is 150; it corresponds to a Reynolds number of about 2270 based on the bulk-mean velocity, U_{ave}, and the channel depth, δ. The Prandtl number (Pr) is 1 in these computations. This value of the Prandtl number is much smaller than that in pure water at standard pressure and temperature ($Pr \approx 5.11$ at 273 K and 101.3 kPa). Since the characteristic length scale of the fluctuating temperature field is much smaller than that of velocity fields when the Prandtl number is larger than 1, DNS of fluids with a high Prandtl number requires huge CPU resources. Therefore the assumption of $Pr = 5$ is not acceptable numerically with the current resolution. Mètais and Herring (1989) conducted a DNS of freely evolving stably stratified turbulence using the assumption of $Pr = 1$. They compared their DNS data with measurements in saltwater (Itsweire et al., 1986). The experimental Prandtl number in saltwater is about 200; however, the DNS data agree well with the measurements. Mètais and Herring (1989) concluded that the large-scale structures are quite similar in both the DNS and the experiments. Although the Prandtl number plays an important role in the dynamics of turbulence in the stably stratified flows, the Prandtl number effect is not significant for the large-scale motions in weakly stratified turbulence. In this article, we concentrate on describing the large-scale motions in the stably stratified free-surface flows for $Pr = 1$ in the weakly stratified flows. Later we will show the influence of the Prandtl number on the transport properties in stably stratified flows to compare the present predictions with the previously published results. Table 1 shows the parameters used in each DNS conducted. The Reynolds number based on the equivalent diameter, $D_{eq} = 4\delta$ in a free-surface flow, and the bulk-mean velocity, U_{ave},

$$Re_D = \frac{D_{eq} U_{ave}}{\nu}, \tag{7}$$

is also used in this article.

Numerical strategy

The computations were carried out with $64 \times 64 \times 65 (= 266,240)$ grid points in the streamwise, spanwise, and vertical directions. The grid spacing in the streamwise and spanwise directions are equidistant and about 14.7 and 7.4 wall units. Grid points are highly concentrated in the vicinity of both the vertical boundaries to capture the rapid variation of velocity, pressure, and temperature there. The minimum and maximum grid spacings in the vertical direction are about 0.39 and 4.74 wall units. The equations are approximated by a finite difference method on a Cartesian staggered grid. This numerical method has a number of practical advantages, for example, ease of implementation and straightforwardness to generalized coordinate systems. The second-order central difference (Harlow and Welch, 1965) is employed to approximate all spatial derivatives.

Table 1. Outline of Computations

Case	Re	Pr	Ri	U_{ave}/u_τ	U_{ave}/u_τ	Ri_b	Re_D
N			0	15.15	17.76	0	9,090
S1	150	1	10	16.83	20.78	0.0351	10,100
S2			20	18.21	23.35	0.0603	11,000

These governing equations are advanced in time by a fractional-step method (Kim and Moin, 1985). The nonlinear and the viscous terms are integrated by a fully explicit second-order Runge–Kutta method (Nagaosa and Saito, 1996). The pressure terms and the divergence of velocity are treated implicitly. The resulting pressure Poisson equation is solved by a direct Poisson solver (Schumann and Sweet, 1989) to reduce CPU time and divergence error. To use this algorithm, the divergence error of the velocity fields is always less than 10^{-12} of $\partial u_i/\partial x_i$.

The computations were carried out for 3,000 viscous time units (tu_τ^2/ν) with a time increment of 0.075 (40,000 time steps) to estimate the fully developed turbulence statistics and other important features of turbulence scalar transport. The nondimensional Courant number defined by

$$C_r(t) = \max\left\{\Delta t\left(\left|\frac{u_1}{\Delta x_1}\right| + \left|\frac{u_2}{\Delta x_2}\right| + \left|\frac{u_3}{\Delta x_3}\right|\right)\right\} \tag{8}$$

stayed below about 0.35 throughout the computations. The computations presented here were carried out on the CRAY Y/MP C90 parallel supercomputer at Research Information Processing Station, Agency of Industrial Science and Technology.

Structure of Unstratified Free-Surface Turbulence

Intercomponent energy transfer near the free surface

As a first step to discuss the structure of free-surface turbulence, fully developed turbulence statistics in an unstratified flow were compared with previously published studies to confirm the suitability of the numerical methods used in this study. We found good agreement with the previous reports of the simulations of free surface turbulence by Lam and Banerjee (1992) and Handler et al. (1993) and the measurements by Komori et al. (1993). We do not show the details of these comparisons in this article. See our previously published report (Nagaosa and Saito, 1996) for detailed discussions of these comparisons.

A shear-free boundary layer is established below the free surface. However, a large part of the structure in the shear-free boundary layer remains unknown because of lack of information. The turbulence energy blocked by the free surface is redistributed to the surface-parallel directions by pressure-strain (Perot and Moin, 1995) in the shear-free boundary layer. Unfortunately the details of the mechanism of intercomponent energy transfer are unknown. Since the effect of shear is not dominant in the boundary layer below the free surface, sophisticated treatment of the pressure strain is required to establish a subgrid scale model. We found that the turbulence intensity in the spanwise direction increases in the vicinity of the free surface at $0.8 < x_3/\delta < 1.0$, as shown in Figure 2. On the other hand, the turbulence intensity in the streamwise direction does not markedly increase, that is, the intercomponent energy transfer is not homogeneous in the two surface-parallel directions. Komori et al. (1993) and Handler et al. (1993) estimated the vertical profiles of the diagonal components of the pressure-strain tensor, defined as

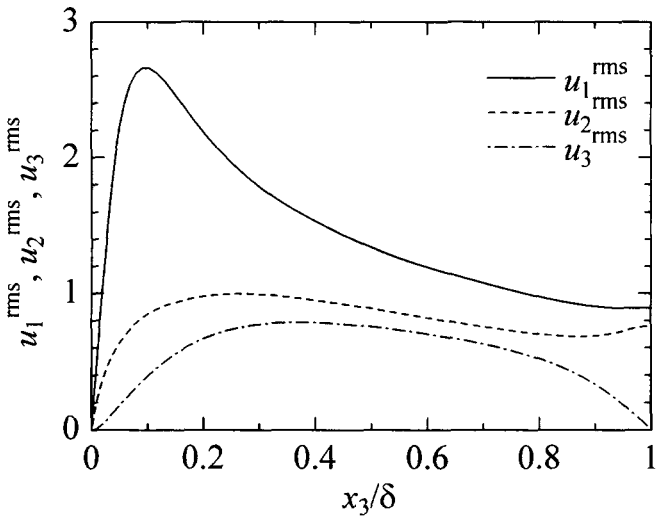

Figure 2. Vertical distributions of turbulence intensities in free-surface flow.

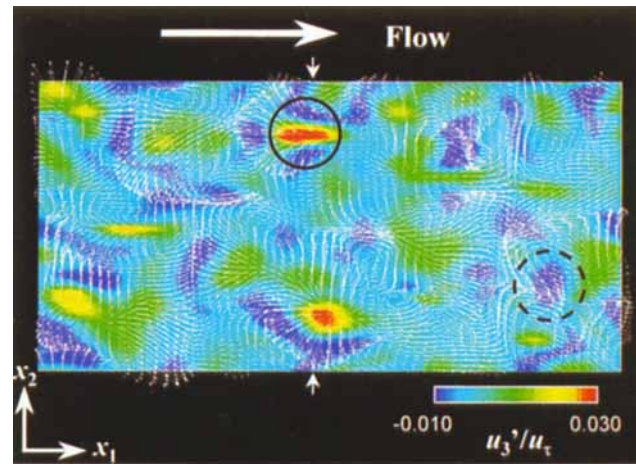

Figure 4. Instantaneous vertical velocity fluctuation near free surface with velocity vectors.

Solid open-circle and dashed open-circle indicate splatting and antisplatting, respectively.

$$\Pi_{ij} = \overline{p'\left(\frac{\partial u_i'}{\partial x_j} + \frac{\partial u_j'}{\partial x_i}\right)}. \qquad (9)$$

The trace of this tensor, Π_{ii}, is always zero because of the incompressible condition. We also estimated the vertical distribution of the pressure-strain terms in the unstratified turbulence as shown in Figure 3. The pressure-strain in the vertical direction, Π_{33}, rapidly decreases near the interface and its sign changes from positive to negative. Π_{22} increases in the vicinity of the free surface and remains positive, while the value of Π_{11} near the interface is much smaller than Π_{22}, and is near zero on the interface. These distributions suggest that the blocked turbulence energy in the vertical direction is mainly transferred into the spanwise direction through the pressure-strain effect. This inhomogeneity in the intercomponent energy transfer in unstratified free-surface turbulence was already reported by Komori et al. (1993) and Handler et al. (1993) in fully developed free-surface flows. Similar distributions of the pressure-strain were also reported by Perot and Moin (1995) and Walker et al. (1996) in decaying turbulence with free-surface. However, these reports did not provide an answer as to why the inhomogeneity exists in the intercomponent energy transfer in the surface-parallel directions.

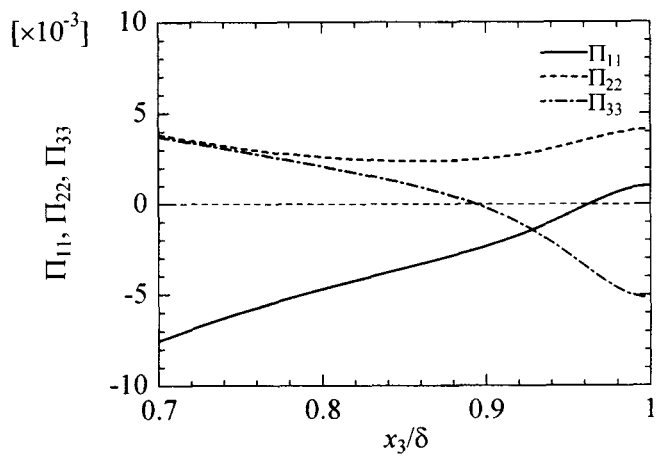

Figure 3. Vertical distributions of pressure-strain terms in unstratified free-surface flow.

To understand this perculiarity of the free-surface turbulence, both velocity and vorticity fields near the free surface are discussed. Figure 4 is a top view of the velocity vectors in the region very close to the free surface, superimposed on a contour map of the instantaneous vertical velocity fluctuation that indicates the activity of the turbulence near the free surface. Splattings, which are at the center of the diverged velocity vectors with a positively large vertical velocity fluctuation, are revealed on the free surface as indicated by a solid open circle in this figure. This structure contributes to the intercomponent energy transfer from vertical to surface-parallel directions. In contrast, antisplattings, which are encountered at the vicinity of converged velocity vectors (indicated by a dashed open circle), exist on the free surface. In the center of the antisplattings, vertical velocity fluctuation is large with downward direction. Antisplattings transfer the turbulence energy from a surface-parallel to a vertical direction. In fully developed free-surface flows, the turbulence energy is mainly transferred from vertical to the spanwise direction in a region close to the free surface. Therefore, we only discuss the turbulence structure around the splattings. In Figure 5, the close-up shot of the spatial vorticity structure around the splattings indicated by the open circle in Figure 4 is shown. We used the streamwise component of the fluctuating voriticity, defined by $\omega_i' = \epsilon_{ijk}\partial u_j'/\partial x_k$, as a vortex indicator. The solid lines in Figure 5 are the streamlines in the $x_2 - x_3$ plane, as indicated by closed white arrows in Figure 4. It is also clear that this organized structure has dipole vorticity, where two vortices are aligned along the streamwise direction. The vertical velocity fluctuation is quite large between these vortices. This positively large vertical velocity region corresponds to the center of the splatting, as indicated in red in Figure 4. The preceding suggests that the splattings are the result of the complicated interaction between these streamwise vortices.

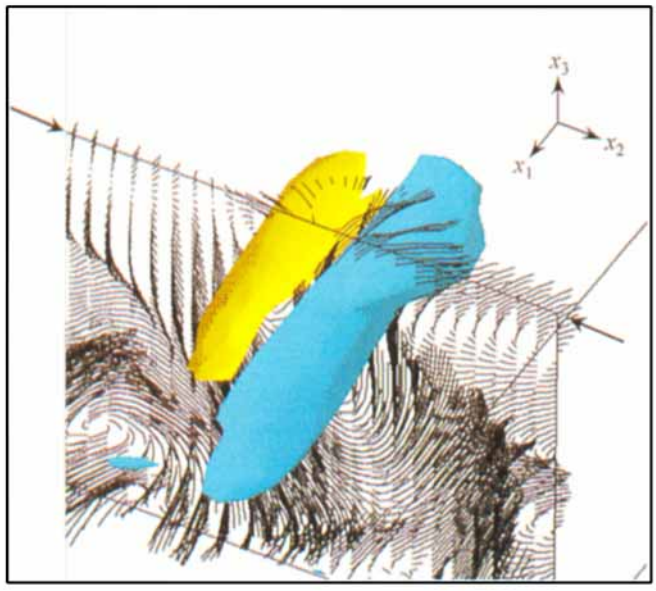

Figure 5. Perspective view of vorticity structure around splatting.

Streamwise component of fluctuating voriticity is used as a vortex indicator. Yellow and blue colors show positive and negative vorticity, respectively.

A simplified sketch of the dynamics of these splattings is shown in Figure 6. The vortices are aligned along the streamwise direction, and therefore cannot transfer turbulence energy to the streamwise direction. Furthermore, it should be noted that downward currents are expected around the splatting, as shown by the dark blue color in Figure 4. The existence of downward currents around the splatting shown schematically in Figure 6 is confirmed in Figure 4. Figure 6 also shows that the splatting replaces the free-surface fluid with fluid from the bulk by the rotating motion of these vortices. This organized structure corresponds to the surface-renewal motion (Komori et al., 1989) or patchy structure (Rashidi et al., 1991) near the free surface.

Structure of Stratified Free-Surface Turbulence

Effect of the molecular Prandtl number

We tried to compare the present predictions with previous measurements in stably stratified free-surface turbulence.

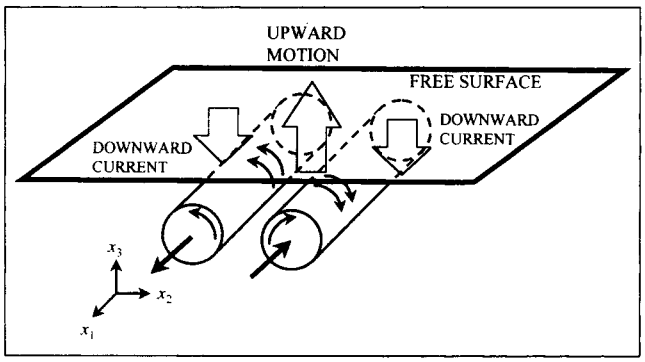

Figure 6. Turbulence structure around splatting.

However, no data were available except the measurements by Komori et al. (1983) in the stably stratified water channel at $Pr = 5$. Komori et al. measured the turbulence statistics and correlated their data with the local Richardson number, defined as

$$Ri_\ell = \beta g \frac{(\partial \overline{T}/\partial x_3)}{(\partial \overline{u_1}/\partial x_3)^2}. \tag{10}$$

Their purpose was to understand the details of the structure of stably stratified homogeneous turbulence; therefore, only the measurements in the region at $0.45 < x_3/\delta < 0.75$ were shown in their report. We can also confirm that the assumption of homogeneous shear flow is fairly satisfied in this region. Gerz et al. (1989) performed a DNS of homogeneous shear flows in air ($Pr = 0.7$) and water ($Pr = 5$) and compared the data with the results of Komori et al. (1983, Figure 5) to justify their DNS data. We also show their results superimposed in our data for comparison. Note that these comparisons do not provide critical testing because the results by Komori et al. (1983) and Gerz et al. (1989) do not perfectly cover the condition of our numerical simulations.

Figure 7 shows the turbulence statistics estimated in the stratified free-surface turbulence at $0.4 < x_3/\delta < 0.75$ together with the results from Komori et al. (1983) and Gerz et al. (1989). Note that the molecular Prandtl number is 1 in our study. The data obtained by Komori et al. (1983) are scattered among individual experimental runs, and quantitative comparisons with our data are difficult. In addition the plots of our data in Figure 7 do not cover the wide Ri_ℓ criterion. We can only say that the results of this study agree with those of previous studies, although the Prandtl number and the flow field are different for each study. The results of this study show especially good agreement with the results of Gerz et al. (1989) for $Pr = 0.7$, since the Prandtl number used here ($Pr = 1$) is very close to that used in their study. Figure 7 also shows that the effect of the molecular Prandtl number is especially important for the distributions of correlation coefficients between u_3' and T' and the ratio of the vertical and streamwise eddy diffusivities, $-\overline{u_3'T'}/\overline{u_1'T'}$, in strongly stratified turbulence of $Ri_\ell > 0.25$. In the high local Richardson number region of $Ri_\ell > 0.25$, these turbulence statistics become negative in water ($Pr = 5$). These negative statistical values show the existence of countergradient heat flux in the vertical direction. In contrast, the closed square plots in Figure 7d and 7e indicate that these statistics are always positive in the region $0 < Ri_\ell < 0.5$ in air ($Pr = 0.7$). The countergradient heat flux in the high local Richardson number region is not predicted in the present assumption at $Pr = 1$. This assumption only gives an overestimation of $-\overline{u_3'T'}/u_3^{\mathrm{rms}}T^{\mathrm{rms}}$ and $-\overline{u_3'T'}/\overline{u_1'T'}$ for $0 < Ri_\ell < 0.25$. The assumption of $Pr = 1$ in this numerical simulation was also used by Mètais and Herring (1989) to compare their data with the measurements by Itsweire et al. (1986) at $Pr = 200$. The comparisons between the numerical results and the measurements were relatively good.

We conclude that the effect of the Prandtl number on the turbulence structure is generally dominant. However, the effect of the Prandtl number on the structures of the large-scale motions is not large, particularly in the weakly stratified flows

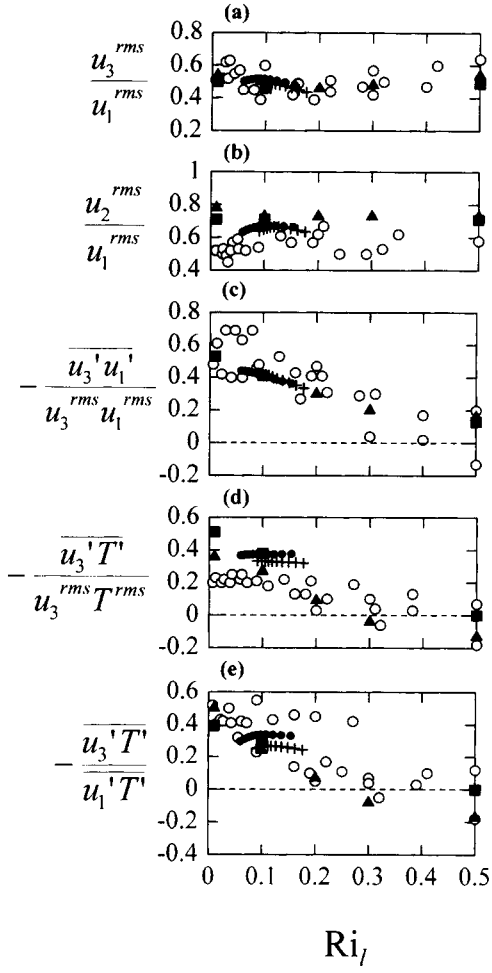

Figure 7. Fully developed turbulence statistics in stably stratified free-surface flows.

●●●●, Case S1; + + + +, Case S2, ○, Komori et al. (1983) in water ($Pr = 5$); ▲, Gerz et al. (1989) in water ($Pr = 5$); ■, Gerz et al. (1989) in air ($Pr = 0.7$).

of $0 < Ri_\ell < 0.25$. The structure of fine-scale motions is mainly emphasized in high Prandtl number fluids ($Pr > 1$), rather than in low Prandtl number fluids ($Pr < 1$). From this point of view, we do not consider the countergradient heat flux in this article, since the countergradient heat flux occurs at the high wave-number region in liquid (Komori and Nagata, 1996). The effect of stable stratification on turbulence structure at a low Ri_ℓ criterion, and not high Ri_ℓ, was discussed in the preceding sections.

Dissociation of the streaklike structure in turbulent boundary layer

Figure 8 shows the mean velocity profiles in stably stratified flows. It should be noted that these velocity profiles are much larger than for unstratified flows, especially in the region at $30 < x_3^+ < 150$. Clearly, the bulk-mean velocity increases with increasing Richardson number, although the friction velocity on the bottom wall is not changed. This is evidence that the turbulent boundary layer is relaminarized in stably stratified flows.

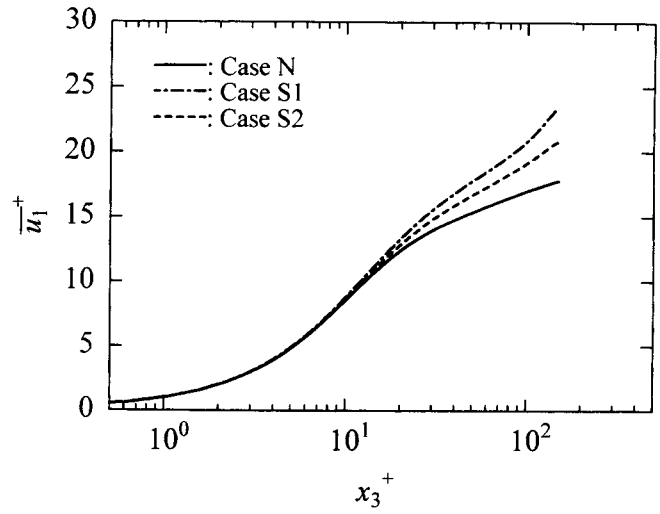

Figure 8. Mean velocity profiles in stably stratified free-surface flows.

The skin friction coefficient, defined by $C_f = \tau_w/(1/2)\rho U_{ave}^2$, is a suitable measure for discussing the global variation of the turbulence structure in the turbulent boundary layer above the rigid wall, since this parameter is sensitive to the variation of the turbulence structure in the boundary layer. The skin friction coefficient and the hydraulic Reynolds number are shown in Table 2. The skin friction coefficient for $Ri = 0$ ($C_f = 8.71 \times 10^{-3}$) is in good agreement with the correlation by Dean (1978), $C_f = 8.89 \times 10^{-3}$. Komori et al. (1989) used the Blasius equation, $C_f = 0.0791 Re_D^{-1/4}$, to estimate the friction velocity, but it underestimates the skin friction coefficient, $C_f = 8.10 \times 10^{-3}$. Nevertheless, this discrepancy (about 11%) is within the permissive error in engineering.

The imposition of the stable stratification is quite effective in reducing the skin friction. The skin friction coefficient for $Ri = 20$ is about 70% that for $Ri = 0$. Figures 9a, 9b, and 9c show the vertical distribution of the turbulence intensities relative to the bulk-mean velocities in streamwise, spanwise, and vertical directions. In the turbulent boundary layer above the rigid wall, the turbulence intensities in each direction considerably decrease due to the stable stratification. It is well known that the turbulent boundary layer is relaminarized by body forces, for example, buoyancy force or coriolis force. The relaminarization of turbulent boundary layer is characterized by the drag reduction, decrease of turbulence intensity relative to the free stream velocity and other features of turbulence statistics distributions. From the distributions of the turbulence statistics, the structure of the turbulent boundary layer above the rigid wall is considerably affected by the stable stratification.

The positive deviation of the mean velocity profiles as shown in Figure 8 is also observed in the turbulent boundary

Table 2. Skin Friction Coefficients in the Stably Stratified Free-Surface Flow

Case	Ri	Re_D	C_f
N	0	9,090	8.71×10^{-3}
S1	10	10,100	7.06×10^{-3}
S2	20	11,000	6.03×10^{-3}

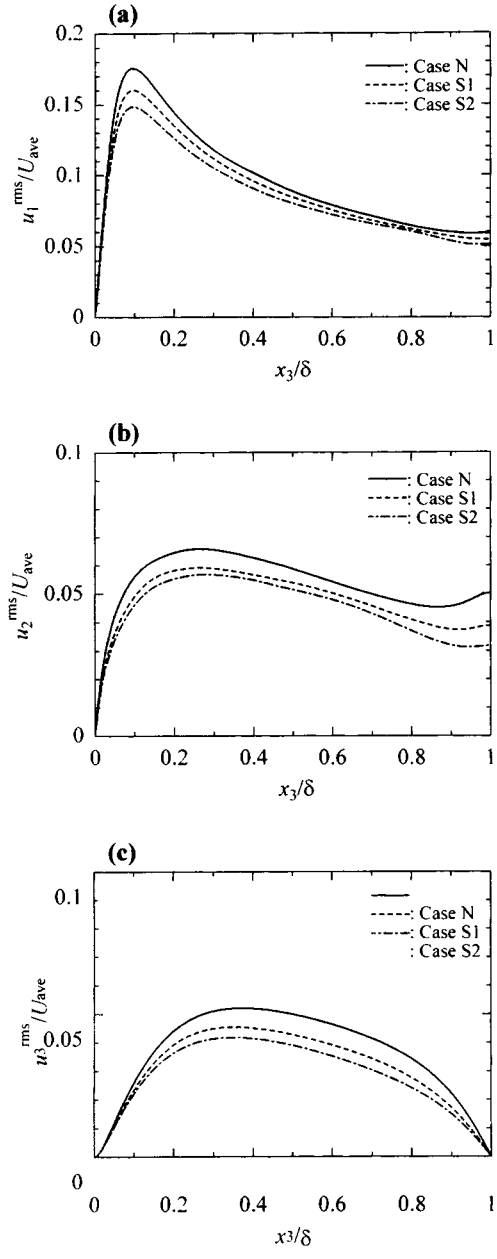

Figure 9. Vertical distributions of turbulence intensities in both unstratified and stratified flows.

(a) Streamwise direction; (b) spanwise direction; (c) vertical direction.

layer above a drag-reductive riblet-mounted wall (Chu and Karniadakis, 1993; Choi et al., 1993). In addition to the positive deviation of the bulk-mean velocities, the decrease of the maximum Reynolds stress is also revealed above the riblets (Choi et al., 1993). The decrease of the maximum Reynolds stress on the riblets is quite rational, because the drag reduction that is accomplished on the riblets will restrict the generation of the organized motion in the boundary layer. The same trend in the Reynolds stress profiles is also observed in the stratified turbulent boundary layer, as shown in Figure 10. The mechanism of the drag reduction in stratified flows is different from that in the riblet-mounted boundary layer. In the turbulent boundary layer with riblets, the interaction of

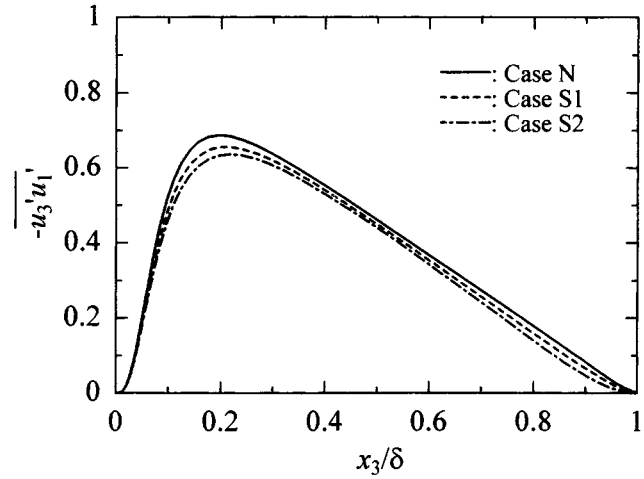

Figure 10. Vertical distribution of Reynolds stress in both unstratified and stratified free-surface flows.

the quasi-streamwise vortices (organized motions) and the wetted surface is highly limited by the presence of the small-spacing riblets (Choi et al., 1993). In the case of the stably stratified turbulent boundary layers, the mechanism of drag reduction is strongly connected to the buoyancy effect. It is interesting that we can see that similar behavior of the turbulence statistics distributions is observed in both the riblet-mounted and stably stratified boundary layer although the mechanism of the drag reduction is quite different. We discuss the mechanism of the drag reduction in the stratified turbulent boundary layer from the viewpoint of internal energy conversion.

A large part of the turbulence energy production in the turbulent boundary layer is due to the quasi-streamwise vortices, which are the typical coherent structures in the wall turbulence. Therefore, the streak formation or dissociation is one of the measures for drag reduction in the turbulent boundary layer. Figure 11 shows the contour maps of the streamwise component of the instantaneous velocity fluctuation at $x_3^+ \approx 10$ in both unstratified and stratified turbulent boundary layers. The formation of streaks is clearly suppressed with increasing Richardson number. This result also suggests that the turbulent boundary layer is relaminarized when stable stratification is imposed. The mechanism of the relaminarization can be explained by internal energy conversion between the turbulent kinetic energy and the potential energy. The low-temperature (heavy) fluid cannot obtain enough turbulence kinetic energy from the high-temperature (light) fluid flowing into it, or the high-temperature fluid consumes much more turbulence kinetic energy to lift the low-temperature fluid. The important processes of bursting, ejection, and sweep, consist of strong vertical motions, therefore, the presence of stable stratification suppresses the generation of bursting motions in the near-wall turbulent boundary layer. According to Komori et al. (1989, 1990), about 90% of bursting eddies generated in the near-wall turbulent boundary layer evolve the surface-renewal motions. The dissociation of the streaklike structures in the near-wall region means that the frequency of the bursting eddies decreases in the stably stratified wall turbulence (Hinze, 1975). We expect that

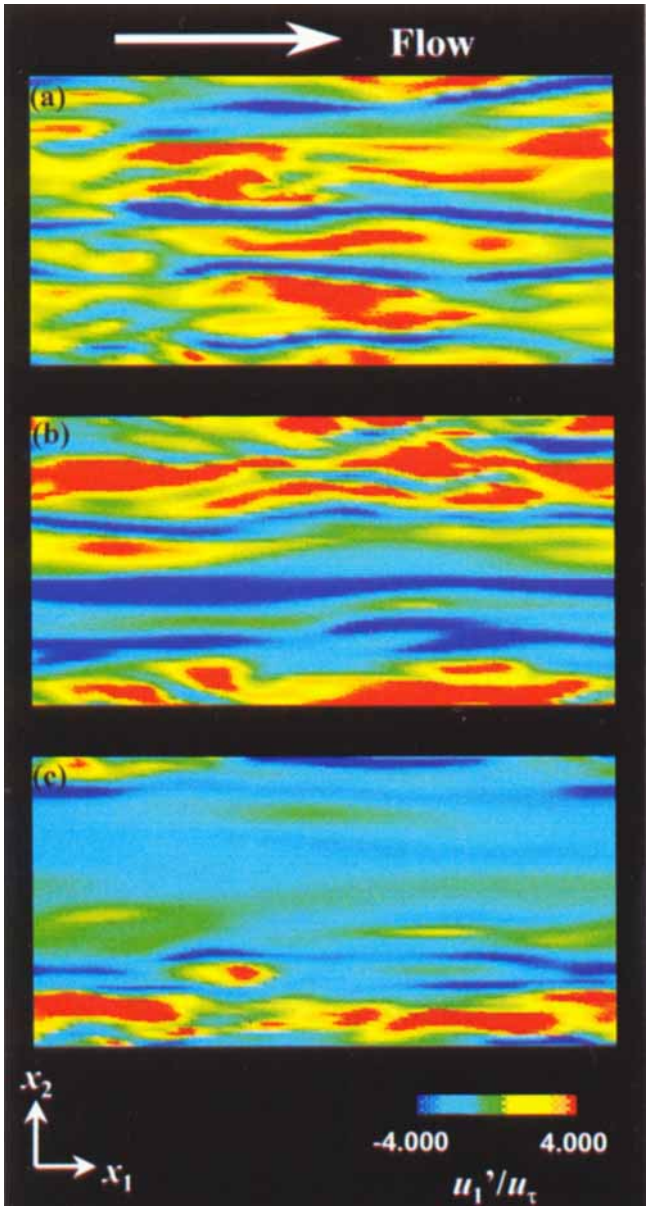

Figure 11. Streaky structure in turbulent boundary layer at about $x_3^+ \approx 10$.

(a) Case N ($Ri = 0$); (b) Case S1 ($Ri = 10$); (c) Case S2 ($Ri = 20$).

the frequency of the surface-renewal motions also decreases because of the stable stratification. In the next section, we discuss the turbulence structure in the region close to the free surface.

Influence of the stable stratification on the turbulence structure near the free surface

The structure-renewal motions are mainly generated in the turbulent boundary layer above the rigid wall when the stable stratification is not imposed (Komori et al., 1989). This strong interaction between the organized structure in the turbulent boundary layer and the surface-renewal motions near the free surface is also observed in the stratified flows in our DNS. We think that the renewal of the free surface is highly reduced in the stratified free-surface turbulence because of the dissociation of the streaks shown in Figure 11. Figure 12 shows contour maps of the instantaneous vertical velocity fluctuation, with streamlines, looking down at the free surface in both the unstratified and stratified flows. The red and yellow colors indicate a large, positive vertical velocity fluctuation, and the blue and green signify a negative vertical velocity. When stable stratification is not imposed, active turbulence motions appear on the free surface. The replacement of the fluid elements due to the surface-renewal motion is very active in the $Ri = 0$ case. From these visualizations, it can be seen that the turbulence structure near the free surface is remarkably affected by the stable stratification.

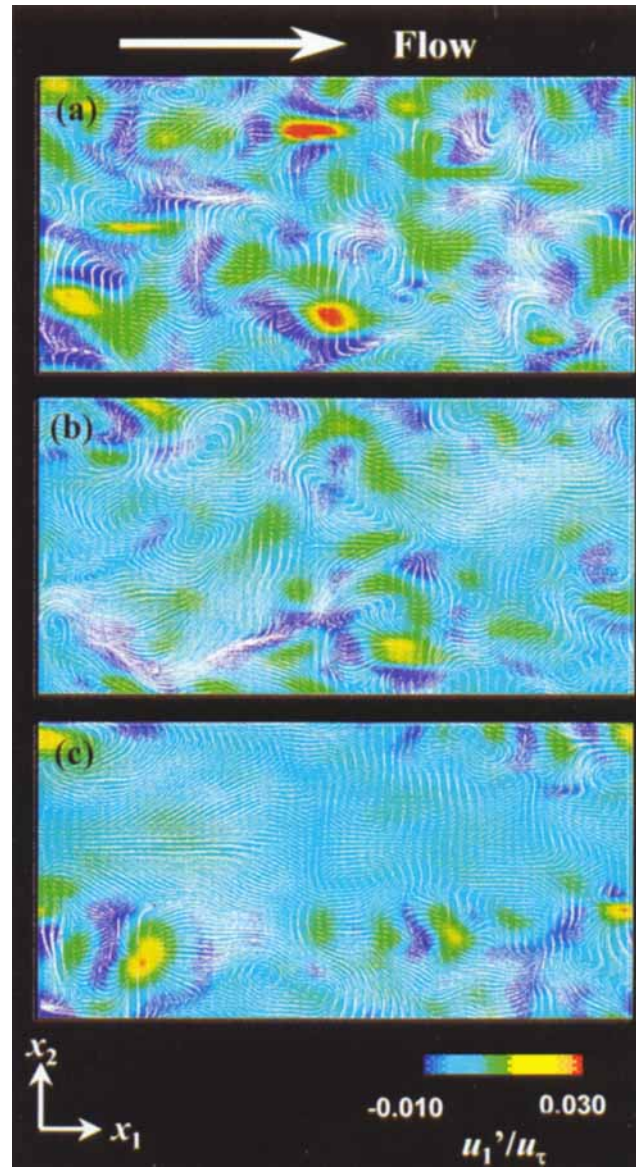

Figure 12. Contour maps of instantaneous vertical velocity fluctuation superimposed on streamlines.

(a) Case N ($Ri = 0$); (b) Case S1 ($Ri = 10$); (c) Case S2 ($Ri = 20$).

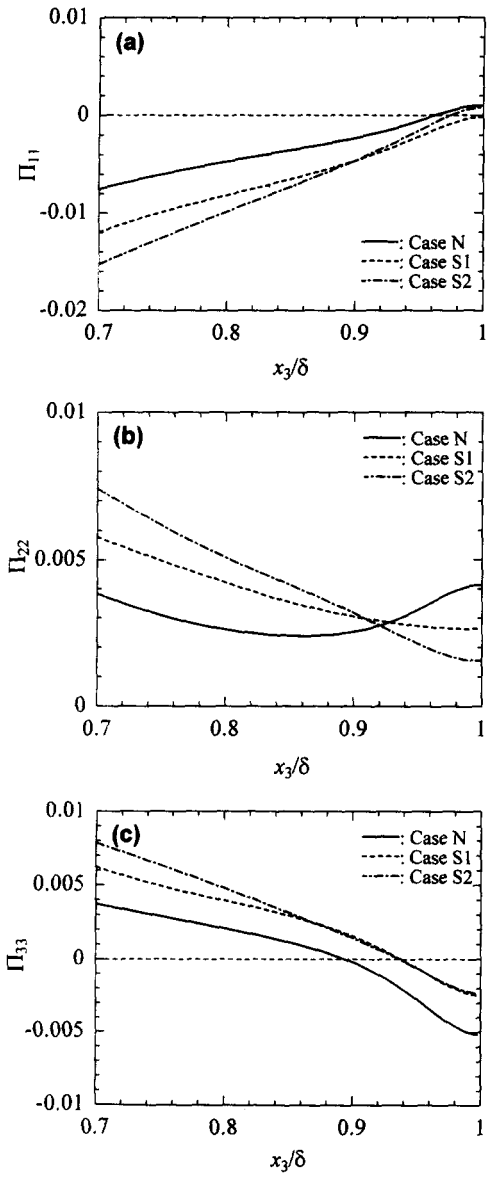

Figure 13. Vertical distributions of pressure-strain terms in both unstratified and stratified free-surface flows.

(a) Streamwise direction; (b) spanwise direction; (c) vertical direction.

Figure 13 shows the vertical distributions of the pressure-strain terms in both the unstratified and stratified cases. The absolute values of Π_{22} and Π_{33} at the free surface decrease with increasing Richardson number. These pressure-strain profiles indicate that the intercomponent energy transfer between the vertical and spanwise directions is deactivated in stratified flows. As described earlier, the turbulent boundary layer is relaminarized by the stable stratification. Most of the surface-renewal eddies are originally generated in the turbulent boundary layer above the rigid wall. Therefore, the depression of the surface-renewal motions near the free surface is a direct result of the relaminarization of the turbulent boundary layer. Consequently, the intercomponent energy transfer is deactivated.

Scalar Transfer across the Free Surface

Scalar transfer coefficient

To deduce the relation between scalar transfer across the free-surface and the turbulence structure in the stratified flows, the unsteady passive scalar transport equation,

$$\frac{\partial C}{\partial t} = -\frac{\partial}{\partial x_j} u_j C + \frac{1}{ReSc} \frac{\partial^2 C}{\partial x_j \partial x_j}, \tag{11}$$

is solved after both the velocity and temperature fields are fully developed. We also assume that the Schmidt number, $Sc = \nu/D$, is equal to unity in the same way as the Prandtl number. The boundary conditions on both vertical boundaries are

$$\frac{\partial C}{\partial x_3} = 0 \quad \text{at} \quad x_3 = 0,$$

$$C = C_0 \quad \text{at} \quad x_3 = \delta. \tag{12}$$

The boundary condition on the bottom wall means no scalar flux exists at the bottom wall. Periodicity is assumed in the two surface-parallel directions.

The scalar transfer coefficient is estimated from the computed scalar field,

$$k_L(t) = \frac{D}{L_1 L_2 (C_0 - C_b)} \int_0^{L_1} \int_0^{L_2} \left(\frac{\partial C}{\partial x_3} \right)_{\text{free surface}} dx_1 dx_2. \tag{13}$$

Since the periodic boundary condition is also used in both the streamwise and spanwise directions with the adiabatic bottom-wall condition, the computations have to be ended before the passive scalar accumulates in the computational domain. The concentration on the bottom wall is always monitored to decide whether accumulation of the passive scalar occurs or not. As a preliminary check, we computed the long-time evolution of the passive scalar field in the unstratified flow. The concentration of the bottom wall gradually increases after about $t^+ = tu_\tau^2/\nu = 150$. Then the evolution of the scalar transient coefficient saturates with small oscillation at about $t^+ = 225$. After this time the variation of the scalar transfer coefficients lie within 3%. At this time, concentration on the bottom wall is about 4% compared to that on the free surface. Therefore, the scalar transfer coefficient is estimated at $t^+ = 225$.

The scalar transfer coefficients are scaled by the channel depth and the molecular diffusivity, giving the Sherwood number,

$$Sh = \frac{k_L \delta}{D}. \tag{14}$$

Figure 14 shows the evolution of the Sherwood number at the free surface. In the earlier stage of $t^+ < 100$, the evolution of the Sherwood numbers do not show any remarkable difference. This means that the transport due to turbulence is not dominant in the earlier stage of the scalar transfer. The effect of the stable stratification is gradually revealed

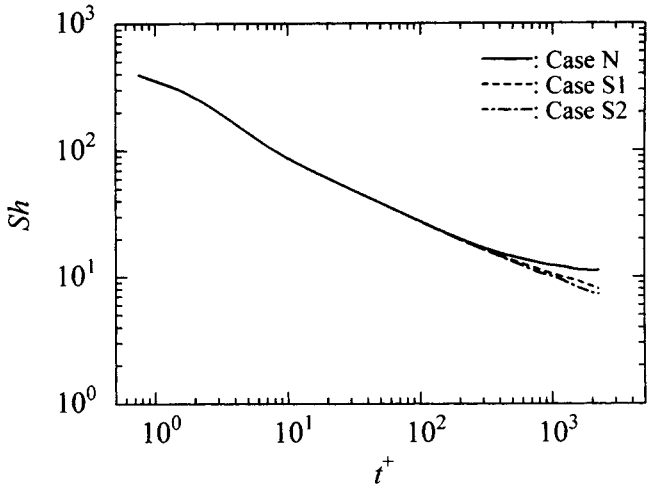

Figure 14. Evolution of Sherwood numbers in both unstratified and stratified free-surface flows.

after about $t^+ = 100$. Clear Richardson number dependency of the scalar transfer coefficients is observed. The scalar transfer coefficient decreases with increasing Richardson number. This results from the deactivation of the surface-renewal motions near the free surface.

Comparisons of the measurements

We calculate the Sherwood number from Eqs. 13 and 14 using the computed scalar fields and correlate it with the hydrodynamic Reynolds number in Figure 15. It is evident that increasing the Reynolds number in the stable stratification does not activate the scalar transfer across the free surface. It seems not to be reasonable. However, it should be noted that the reduction of the scalar transfer coefficient in the stratified free-surface flows is quite rational because the surface-renewal motions are dissociated, as shown in Figure 12. Concerning the decrease of the Sherwood number in spite of the increase in the Reynolds number, the following mechanism is suggested:

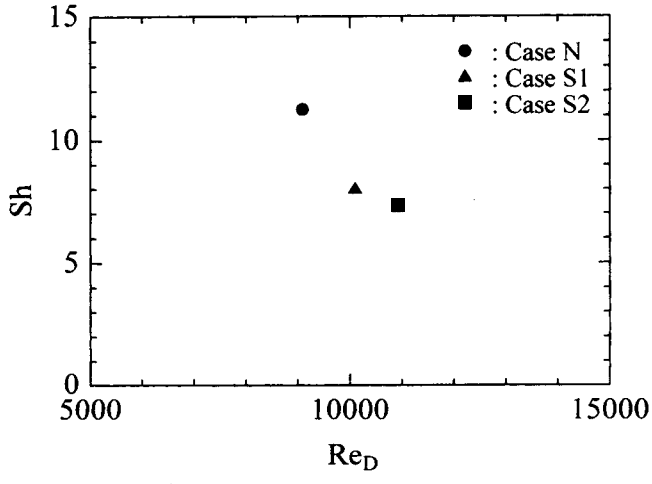

Figure 15. Sherwood number vs. Reynolds number.

1. The organized motions in the stratified turbulence are dissociated.
2. The effect of the stable stratification relaminarizes the turbulent flow in the open-channel flow.
3. Bulk-mean velocity increases due to the relaminarization of the turbulence.
4. However, the scalar transfer coefficient decreases with increasing the Richardson number, since the organized motions are dissociated.

It further indicates that the scalar transfer rate in the stably stratified flows is strongly influenced by the Richardson number, rather than the Reynolds number. Note that the increase of the Reynolds number is a result of the increase of the Richardson number; therefore, the scalar transfer is not enhanced in the stably stratified flows.

Quantitative discussions of the scalar transfer are required for predicting the scalar transfer rate in the stratified free-surface turbulence. As a first step, the scalar transfer coefficient in the unstratified flows is discussed. Rashidi et al. (1991) and Komori et al. (1989) studied the relationship between the scalar transfer coefficient, k_L, across the free surface and the turbulence quantities in the unstratified free-surface turbulence with an unsheared flat gas–liquid interface. Their results are as follows:

$$\frac{k_L Sc^{1/2}}{(u_\tau U_{ave})^{1/2}} = 7.7\times10^{-3} \qquad \text{(Rashidi et al.)} \qquad (15)$$

$$k_L = 0.34(Df_s)^{1/2}, \qquad \frac{f_s\delta}{U_{ave}} = 4.7\times10^{-5}Re_D^{0.85},$$

(Komori et al.) (16)

Using Dean's correlation for the skin-friction coefficient (Dean, 1978),

$$C_f = 0.0868\,Re_D^{-1/4}, \qquad (17)$$

in Eq. 15, we can obtain a general relationship between the hydrodynamic Reynolds number and the Sherwood number,

$$ShSc^{1/2} = \begin{cases} 1.01\times10^{-3}Re_D^{0.93} & \text{(Rashidi et al.)} \\ 1.11\times10^{-3}Re_D^{0.93} & \text{(Komori et al.).} \end{cases} \qquad (18)$$

The predicted Sherwood numbers using Eq. 18 are shown in Table 3 when $Sc = 1$ is assumed. Equations 18 involve the external correlation (e.g., Eq. 17); therefore, original mea-

Table 3. Comparison of the Sherwood Numbers Obtained by the DNS

	Re_D	Sh ($Sc = 1$)	k_L (m/s) ($Sc = 600$)
Present DNS	9,090	11.3	9.23×10^{-6}
Prediction by Rashidi et al. (1991)		4.85	4.64×10^{-6}
Prediction by Komori et al. (1989)		5.35	4.40×10^{-6}

surements by Komori et al. (1989) and Rashidi et al. (1991) are directly compared with the results of the DNS and are also shown in Table 3. To consider the difference of the Schmidt number, we assumed that the mass transfer coefficient is proportional to $Sc^{-1/2}$ (i.e., $k_L Sc^{1/2} = \text{const.}$) as shown in Eqs. 18. Hence, the DNS data are easily compared with the measurements, although the Schmidt number is different. For the comparison, $u_\tau = 3.0\times10^{-3}$ m/s, $\delta = 5.0\times10^{-2}$ m, and $\nu = 1.0\times10^{-6}$ m^2/s are assumed to obtain the mass-transfer rate (with dimension) from the results of the DNS. These conditions are close to the measurements by Komori et al. (1989).

The discrepancies between the computed Sherwood number and the predicted values by Eqs. 18 can be found. The computed Sherwood number using this DNS is about 100% larger than the values predicted by Eqs. 18. Unfortunately, we cannot give the reasons why the discrepancies between the results of our simulations and the measurements by Komori et al. (1989) and Rashidi et al. (1991) exist. We can only say that the scalar transfer across the free surface is very sensitive to the chemical condition of the free surface, for example, surface contamination or surface tension due to surfactant (Golovin, 1992; Kim et al., 1996). It will affect the scalar transfer rate at the free surface through variation of the fine-scale motions, for example, Marangoni convection (Golovin, 1992). We consider it necessary to carry out an investigation of the relationship between the scalar transfer rate and the condition of the free surface to use a molecular dynamics simulation.

Conclusions

Direct numerical simulation of stably stratified free-surface flows are carried out with $64\times64\times65$ grid points at a Reynolds number of 150, based on the friction velocity and channel depth. We investigated the relation between the turbulence structure and scalar transfer in stably stratified flows. The results of this study are summarized below.

The intercomponent energy transfer is clearly observed in the unstratified free-surface turbulence. This energy transfer is not homogeneous in the two surface-parallel directions due to the presence of dipole streamwise vortices. These vortices contribute to the surface renewal at the free surface and control the scalar transfer there.

We further investigate the structure of the turbulent boundary layer near the bottom wall because almost all surface-renewal motions are generated in the near-wall region. The turbulent boundary layer is relaminarized when stable stratification is involved. This phenomenon can be confirmed by dissociation of the streaky structures and drag reduction in the turbulent boundary layer. The drag reduction means that the generation of the bursting eddies are reduced in the turbulent boundary layer. The scalar transfer across the free surface is deactivated by the presence of stable stratification because the relation between the bursting frequency and the surface-renewal frequency is quite large.

The Sherwood number at the free surface obtained by our simulations is compared with the measurements by Komori et al. (1980) and Rashidi et al. (1991). We find a large discrepancy between the results of our DNS and their measurements. We point out that the chemical condition of the free surface will be dominant when the scalar transfer rate is measured. We should carry out further investigations to clarify the effect of the chemical condition of the free surface on turbulence structure and scalar transfer. Molecular dynamics simulation will be one of the powerful tools in investigating this relationship.

Acknowledgments

A part of this study is supported by the Fundamental Research Program of the National Institute for Resources and Environment. We thank Dr. Guttorm Alendal at the Nansen Environmental and Remote Sensing Center for his helpful comments and suggestions on the draft of this manuscript. The suggestions of Prof. M. Kawaji of the University of Toronto were of benefit in improving this manuscript. We also thank Prof. T. Kajishima of Osaka University for his helpful advice concerning the numerical schemes used in this study.

Notation

C = concentration
C_0 = concentration at the free surface
C_b = concentration at the bottom wall
D = molecular diffusivity
f_s = frequency of surface-renewal eddies
g = gravitational acceleration
p = pressure
Ri_b = bulk Richardson number $= (u_\tau/U_{ave})^2 Ri$
U_{surf} = mean streamwise velocity on free surface
x_i = spatial coordinates
α = thermal diffusivity
β = volume expansion coefficient
γ = inclination angle of open-channel
Δx_i = grid spacing
Δt = time increment
ϵ_{ijk} = Eddington's epsilon
ρ = density
τ_w = viscous shear stress on bottom wall

Specific symbols

rms = root-mean squared value
$'$ = fluctuating component
$-$ = long-time spatially averaged value
$+$ = value normalized by friction velocity

Literature Cited

Choi, H., P. Moin, and J. Kim, "Direct Numerical Simulation of Turbulent Flow over Riblets," *J. Fluid Mech.*, **255**, 503 (1993).
Chu, D. C., and G. E. Karniadakis, "A Direct Numerical Simulation of Laminar and Turbulent Flow over Riblet-Mounted Surface," *J. Fluid Mech.*, **250**, 1 (1993).
Dankwerts, P. V., "Significance of Liquid-film Coefficients in Gas Absorption," *Int. Eng. Chem.*, **43**, 1460 (1951).
Dean, R. B., "Reynolds Number Dependence of Skin Friction and Other Bulk Variables in Two-Dimensional Rectangular Duct Flow," *J. Fluid Eng.*, **100**, 215 (1978).
Fortesque, G. E., and J. R. A. Pearson, "On Gas Absorption into a Turbulent Liquid," *Chem. Eng. Sci.*, **22**, 1163 (1967).
Gerz, T., U. Schumann, and S. E. Elgobashi, "Direct Numerical Simulation of Stratified Homogeneous Turbulent Shear Flows," *J. Fluid Mech.*, **200**, 563 (1989).
Golovin, A. A., "Mass Transfer under Interfacial Turbulence: Kinetic Regularities," *Chem. Eng. Sci.*, **47**, 2069 (1992).
Harlow, F. H., and J. E. Welch, "Numerical Calculation of Time-Dependent Viscous Incompressible Flow of Fluid with a Free Surface," *Phys. Fluids*, **8**, 2182 (1965).
Handler, R. A., T. F. Swean, Jr., R. I. Leighton, and J. D. Swearingen, "Length Scale and the Energy Balance for Turbulence near a Free Surface," *AIAA J.*, **31**, 1998 (1993).
Hinze, J. O., *Turbulence*, 2nd ed., McGraw-Hill, New York (1975).

Holt, S. E., J. R. Koseff, and J. H. Ferziger, "A Numerical Study of the Evolution and Structure of Homogeneous Stably Stratified Sheared Turbulence," *J. Fluid Mech.*, **237**, 499 (1992).
Itsweire, E. C., K. N. Herrand, and C. W. Van Atta, "The Evolution of Grid-Generated Turbulence in Stably Stratified Fluid," *J. Fluid Mech.*, **162**, 229 (1986).
Jiménez, J., and P. Moin, "The Minimal Flow Unit in Near-Wall Turbulence," *J. Fluid Mech.*, **225**, 213 (1991).
Kim, K. J., N. S. Berman, and B. D. Wood, "Absorption of Water Vapor into LiBr Solutions with 2-Ethyl-1-Hexanol," *AIChE J.*, **42**, 884 (1996).
Kim, J., and P. Moin, "Application of a Fractional-Step Method to Incompressible Navier-Stokes Equations," *J. Comput. Phys.*, **59**, 308 (1985).
Komori, S., H. Ueda, F. Ogino, and T. Mizushina, "Turbulence Structure and Transport Mechanism at the Free Surface in an Open-Channel Flow," *Int. J. Heat Mass Transfer*, **25**, 513 (1982).
Komori, S., H. Ueda, F. Ogino, and T. Mizushina, "Turbulence Structure in Stably Stratified Open-Channel Flow," *J. Fluid Mech.*, **130**, 13 (1983).
Komori, S., Y. Murakami, and H. Ueda, "The Relationship between Surface-renewal and Bursting Motions in an Open-Channel Flow," *J. Fluid Mech.*, **203**, 103 (1989).
Komori, S., and K. Nagata, "Effects of Molecular Diffusivities on Counter-Gradient Scalar and Momentum Transfer in Strong Stable Stratification," *J. Fluid Mech.*, **326**, 205 (1996).
Komori, S., R. Nagaosa, and Y. Murakami, "Mass Transfer into a Turbulent Liquid across the Zero-Shear Gas-Liquid Interface," *AIChE J.*, **36**, 957 (1990).
Komori, S., R. Nagaosa, Y. Murakami, S. Chiba, K. Ishii, and K. Kuwahara, "Direct Numerical Simulation of Three-Dimensional Open-Channel Flow with Zero-Shear Gas-Liquid Interface," *Phys. Fluids A*, **5**, 115 (1993).
Lam, K., and S. Banerjee, "On the Condition of Streak Formation in a Bounded Turbulent Flow," *Phys. Fluids A*, **2**, 1522 (1992).
Mètais, O., and J. R. Herring, "Numerical Simulations of Freely Evolving Turbulence in Stably Stratified Fluids," *J. Fluid Mech.*, **202**, 117 (1989).
Nagaosa, R., and T. Saito, "Direct Numerical Simulation of Turbulence Structure and Heat Transfer across a Free Surface in Stably Stratified Open-Channel Flows," *AIChE Symp. Ser.*, **92**(310), 195 (1996).
Pan, Y., and S. Banerjee, "A Numerical Study of Free-Surface Turbulence in Channel Flow," *Phys. Fluids*, **7**, 1649 (1995).
Perot, B., and P. Moin, "Shear-Free Boundary Layers: 1. Physical Insights into Near-Wall Turbulence," *J. Fluid Mech.*, **295**, 199 (1995).
Rashidi, M., G. Hetsuroni, and S. Banerjee, "Streak Formation and Breakdown near Boundaries in Turbulent Open Channel Flow," *J. Fluids Eng.*, **112**, 164 (1990).
Rashidi, M., G. Hetsuroni, and S. Banerjee, "Mechanisms of Heat and Mass Transport at Gas-Liquid Interfaces," *Int. J. Heat Mass Transfer*, **34**, 1799 (1991).
Schumann, U., and R. A. Sweet, "Fast Fourier Transforms for Direct Solution of Poisson's Equation with Staggered Boundary Conditions," *J. Comput. Phys.*, **74**, 123 (1988).
Walker, D. T., R. I. Leighton, and L. O. Garza-Rios, "Shear-Free Turbulence near a Flat Free Surface," *J. Fluid Mech.*, **320**, 19 (1996).

Manuscript received Sept. 16, 1996, and revision received June 19, 1997.